Somatic *SLC35A2* mosaicism correlates with clinical findings in epilepsy brain tissue

Katherine E. Miller, PhD, Daniel C. Koboldt, MS, Kathleen M. Schieffer, PhD, Tracy A. Bedrosian, PhD,
Erin Crist, MMSc, LGC, Adrienne Sheline, MPH, Kristen Leraas, MS, Vincent Magrini, PhD, Huachun Zhong, MS,
Patrick Brennan, MS, Jocelyn Bush, MS, James Fitch, BS, Natalie Bir, BS, Anthony R. Miller, PhD,
Catherine E. Cottrell, PhD, Jeffrey Leonard, MD, Jonathan A. Pindrik, MD, Jerome A. Rusin, MD,
Summit H. Shah, MD, MPH, Peter White, PhD, Richard K. Wilson, PhD, Elaine R. Mardis, PhD,
Christopher R. Pierson, MD, PhD, and Adam P. Ostendorf, MD

Correspondence
Dr. Ostendorf
Adam.Ostendorf@
nationwidechildrens.org

Abstract

Objective
Many genetic studies of intractable epilepsy in pediatric patients primarily focus on inherited, constitutional genetic deficiencies identified in patient blood. Recently, studies have revealed somatic mosaicism associated with epilepsy in which genetic variants are present only in a subset of brain cells. We hypothesize that tissue-specific, somatic mosaicism represents an important genetic etiology in epilepsy and aim to discover somatic alterations in epilepsy-affected brain tissue.

Methods
We have pursued a research study to identify brain somatic mosaicism, using next-generation sequencing (NGS) technologies, in patients with treatment refractory epilepsy who have undergone surgical resection of affected brain tissue.

Results
We used an integrated combination of NGS techniques and conventional approaches (radiology, histopathology, and electrophysiology) to comprehensively characterize multiple brain regions from a single patient with intractable epilepsy. We present a 3-year-old male patient with West syndrome and intractable tonic seizures in whom we identified a pathogenic frameshift somatic variant in *SLC35A2*, present at a range of variant allele fractions (4.2%–19.5%) in 12 different brain tissues detected by targeted sequencing. The proportion of the *SLC35A2* variant correlated with severity and location of neurophysiology and neuroimaging abnormalities for each tissue.

Conclusions
Our findings support the importance of tissue-based sequencing and highlight a correlation in our patient between *SLC35A2* variant allele fractions and the severity of epileptogenic phenotypes in different brain tissues obtained from a grid-based resection of clinically defined epileptogenic regions.

Glossary

Many genetic epilepsies are characterized by Mendelian inheritance, notably in ion channel genes (e.g., *SCN1/2A*, *KCNQ2*, and *GRIN1/2A/2B/2D*), which also may occur de novo in individuals without any family history of epileptic disorders.[1–3] Approximately one-third of epilepsies are treatment refractory due to failure of medication to alleviate or ameliorate seizures.[4–6] In select cases, electrophysiologic brain mapping can identify affected regions, and the resection or disconnection of these regions is potentially curative. For some patients, the likelihood of becoming seizure-free after surgical resection or disconnection is as high as 80%.[5,6]

Several studies have recently identified somatic mosaicism associated with epilepsy in which genetic variants are present only in a subset of brain cells identified in resected tissue. The most robust association involves genes in the PI3K-AKT-mTOR pathway, wherein hyperactivation of the mTOR pathway occurs in patients with hemimegalencephaly and focal cortical dysplasia (FCD).[7–10] Still, the genetic etiology of many epileptic phenotypes associated with somatic mosaicism remains ill defined.

At Nationwide Children's Hospital, a National Association of Epilepsy Centers Level 4 epilepsy center, we have established a research program to identify brain somatic mosaicism in patients with treatment refractory epilepsy who have undergone surgical resection (figure e-1, links.lww.com/NXG/A273). High-depth next-generation sequencing (NGS) is performed on brain DNA in comparison to blood-derived DNA. Somatic variants are assessed for pathogenicity and analyzed in the context of clinically obtained multimodal information. We hypothesize that tissue-specific, somatic mosaicism represents an important genetic etiology in epilepsy.

Methods

Standard protocol approvals, registrations, and patient consents

This study was designed to perform genomic profiling of excised tissue and matched (blood) samples from a patient with refractory epilepsy. Written informed consent was obtained, and the patient was enrolled as part of an institutional review board-approved research study (IRB18-00786) within The Steve and Cindy Rasmussen Institute for Genomic Medicine at Nationwide Children's Hospital.

Data availability

The *SLC35A2* variant information was deposited in ClinVar (ncbi.nlm.nih.gov/clinvar) under accession number VCV000635117.1.

Histopathology

Hematoxylin and eosin staining was performed as part of routine clinical workup according to recommendations of the International League Against Epilepsy.[11]

Neurophysiology

The index patient underwent multiple extracranial EEG and a single intracranial EEG. All data were digitally acquired and interpreted with a Nihon Kohden system. Interpretations were performed by a board-certified clinical neurophysiologist according to standard clinical care. Quantification of epileptiform activity was performed by counting spikes, polyspikes, and ripples during a 5-minute sample at the beginning of each hour during the last day of recording (120 total minutes from 24 epochs). For each tissue, the correlation between activity (average spikes per minute) and variant allele fraction (VAF) (average tissue VAF from NEBNext Direct [NND]) was calculated in R using the *cor.test* operation.

MRI

The index patient was imaged 3 times before the final diagnosis. The first 2 scans were obtained on a GE Discovery MR750 3T magnet (GE Medical Systems, Milwaukee, WI) using a 32-channel head coil with sedation performed by a pediatric anesthesiologist. The first 2 scans included 3 plane brain volume imaging long inversion recovery (T1 volumetric), axial/coronal T2 FSE, axial susceptibility weighted, and axial diffusion sequences. The second scan also included 3 plane T2 fluid-attenuated inversion recovery (FLAIR) CUBE (T2 volumetric), axial diffusion tensor imaging using 30 gradient encoding directions, and postgadobutrol (Gadovist, Bayer HealthCare, Whippany, NJ) coronal T2 FLAIR, 3 plane brain volume imaging long inversion recovery (T1 volumetric), and axial T1 spin echo sequences. The third MRI scan was performed on a Siemens PRISMA 3T magnet (Siemens, Erlangen, Germany) using a 32-channel head coil with sedation by a pediatric anesthesiologist. The third scan included the following: 3 plane magnetization prepared-rapid gradient ECHO (T1 volumetric), 3 plane T2 FLAIR sampling perfection with application-optimized (T2 volumetric), axial diffusion tensor imaging using 30 gradient encoding directions, axial and coronal T2 high resolution, axial susceptibility-weighted imaging, and postgadobutrol (Gadovist, Bayer HealthCare, Whippany, NJ), coronal T2 FLAIR, 3 plane

magnetization prepared-rapid gradient ECHO (T1 volumetric), and axial T1 spin echo sequences. Interpretations were performed by a board-certified radiologist.

Fluorodeoxyglucose-PET scan

After IV injection of fluorodeoxyglucose (FDG) radiotracer, a PET of the head was performed using a 64-slice GE Healthcare (Chicago, IL) Discovery-690 scanner with the patient under sedation and with simultaneous EEG monitoring. The images were postprocessed and fused with the MRI of the head from the same day using MIM (Cleveland, OH) software.

Surgical resection

The patient underwent a 2-stage epilepsy surgery, whereby stage 1 consisted of insertion of a subdural convexity grid and strip electrodes to identify epileptogenic zones, and stage 2 consisted of a grid-based resection of epileptogenic zones, including the left temporal lobe, left amygdala and hippocampus, left inferior parietal lobe, left occipital lobe, left medial occipital lobe, left inferior parietal cortex, and left superior temporal gyrus. Twelve tissues from different resected brain sections from a singular patient were used for co-DNA/RNA extraction for the purpose of study by NGS (table e-1, links.lww.com/NXG/A273). For frozen samples, we used 30 mg of each tissue for DNA extraction. For formalin-fixed paraffin-embedded (FFPE) samples, we used a calculation to determine the number of scrolls needed based on the total amount of tissue in the block, so the amount of DNA extracted was comparable to all other tissue blocks. DNA extracted from the patient's peripheral blood was used for inherited (germline) variant calling and as a comparator for analysis of acquired (somatic) variants. Intracranial EEG was performed using Ad-Tech (Oak Creek, WI) subdural grid and strip electrodes implanted during a left-sided craniotomy. Electrophysiologic data were digitally recorded using a Nihon Kohden (Tokyo, Japan) digital EEG recording system.

Exome and transcriptome sequencing

DNA extracted from peripheral blood and DNA/RNA from brain resection tissues was used for enhanced exome sequencing using the NEBNext Ultra II FS DNA Library Prep Kit (New England BioLabs, Ipswich, MA). IDT xGen Exome Research Panel v1.0 enhanced with the xGenCNV Backbone Panel-Tech Access (Integrated DNA Technologies, Coralville, IA) was used for target enrichment by hybrid capture. Paired-end 151-bp reads were generated on Illumina HiSeq 4000. Alignment to human reference genome build GRCh37 and secondary analysis was performed using a custom in-house pipeline.[12] Germline variants were called using GATK's HaplotypeCaller, and somatic variants were called using MuTect2.[13,14] Germline variants were filtered based on the following characteristics: GATK quality score (≥30), population frequency (≤ 1%), depth of sequencing (≥8 reads), VAF (≥ 20%), protein-coding region or distance from canonical splice site ≤3 bp, damaging prediction scores (Combined Annotation Dependent Depletion ≥15; Sorting Intolerant From Tolerant ≤0.05; Genomic Evaluationary Rate Profiling++ ≥ 2), and relevance of gene-disease association with patient phenotype using Online Mendelian

Inheritance in Man (OMIM) and ClinVar databases. Candidate germline variants were assessed for pathogenicity according to the American College of Medical Genetics and Genomics (ACMG) and Association for Molecular Pathology (AMP) variant interpretation guidelines.[15]

Somatic variants were filtered based on the following characteristics: MuTect2 = PASS, GATK quality score (≥30), protein-coding region or distance from canonical splice site ≤3 bp, depth of sequencing (≥8 total reads), absence from blood comparator, alternate allele reads (≥5), and VAF (≥1%). Variants passing all criteria were then manually reviewed in Integrated Genomics Viewer (IGV) to assess for strand bias, read-end bias, or other biases, which might suggest sequencing artifacts. Candidate somatic variants were assessed for pathogenicity and for association with epilepsy or a seizure-related phenotype using OMIM and ClinVar databases.

Brain-extracted RNA was subject to DNase treatment and ribodepletion before library construction, using Illumina's TruSeq Stranded total RNA kit. Paired-end 151-bp reads were generated on Illumina HiSeq 4000 and aligned to human reference genome build GRCh38. Alignment and variant calling was performed using a custom in-house pipeline and the splice-aware aligner STAR.[10] Cufflinks (version 2.2.1) was used to generate gene-based Fragments Per Kilobase of transcript per Million mapped reads (FPKM) values for *SLC35A2*. For figure e-2, links.lww.com/NXG/A273: other epilepsy brain tissues were previously resected from patients enrolled on our institutional review board protocol; DESeq2 was used for normalization of expression values, and values for *SLC35A2* were plotted for 6 tissues (A1, A2, B, C, D1, and D2) from the described patient vs brain tissues from other epilepsy patients.[16]

Targeted sequencing

Genomic DNA (10 ng) was used as a template for PCR. *SLC35A2* primers: forward (5′-AGCCTGAGCTGCCTTTG-3′) and reverse (5′- CGGCCACTGGATCAGAAC-3′). PCR was performed using 2x Q5 MM (New England BioLabs) and 200 nM primers with the following conditions: 30″ at 98°C, 30 cycles of 10″ at 98°C, 20″ at 58°C, 20″ at 72°C, and a final extension of 5′ at 72°C. Amplified products were purified using 1.8X SPRIselect, followed by end-repair and dA-tailing using NEBNext Ultra II DNA Library Prep kit reagents. The reaction was followed by adapter ligation with unique molecular identifier (UMI)-IDT-indexed adaptors (Integrated DNA Technologies). Adaptor-ligated samples were purified using 1.2X SPRIselect and used for library amplification with Q5 MM and Illumina P5/P7 primer mix. A post-PCR 1.2X SPRIselect cleanup was performed, and libraries were pooled and sequenced on Illumina HiSeq4000.

NND is a hybridization-based, target-enrichment approach for direct sequencing of region(s) of interest.[17] We used a custom-designed kit targeting coding regions of *SLC35A2* for deep sequencing of DNA and RNA. We used 100 ng (frozen tissue DNA and blood DNA), 200 ng (frozen tissue

RNA), or 500 ng (FFPE tissue DNA). For RNA libraries, double-stranded cDNA was synthesized using high-capacity cDNA reverse transcript kit for first strand (Thermo Fisher Scientific and Applied Biosystems), followed by NEBNext Ultra II nondirectional RNA second strand synthesis kit (New England BioLabs Inc.). The protocol was then followed according to the manufacturer's suggestions, which incorporated unique dual indexes with a UMI next to the i5 index. DNA libraries were sequenced on Illumina iSeq, whereas cDNA libraries were sequenced on Illumina MiniSeq. NND demo pipeline was used for data processing (github.com/DirectedGenomics/DemoPipeline). The raw, deduplicated BAM files were used with SAMtools mpileup and mpileup2cns VarScan (version 2.3.4) commands to generate read counts for our variant of interest.[18,19]
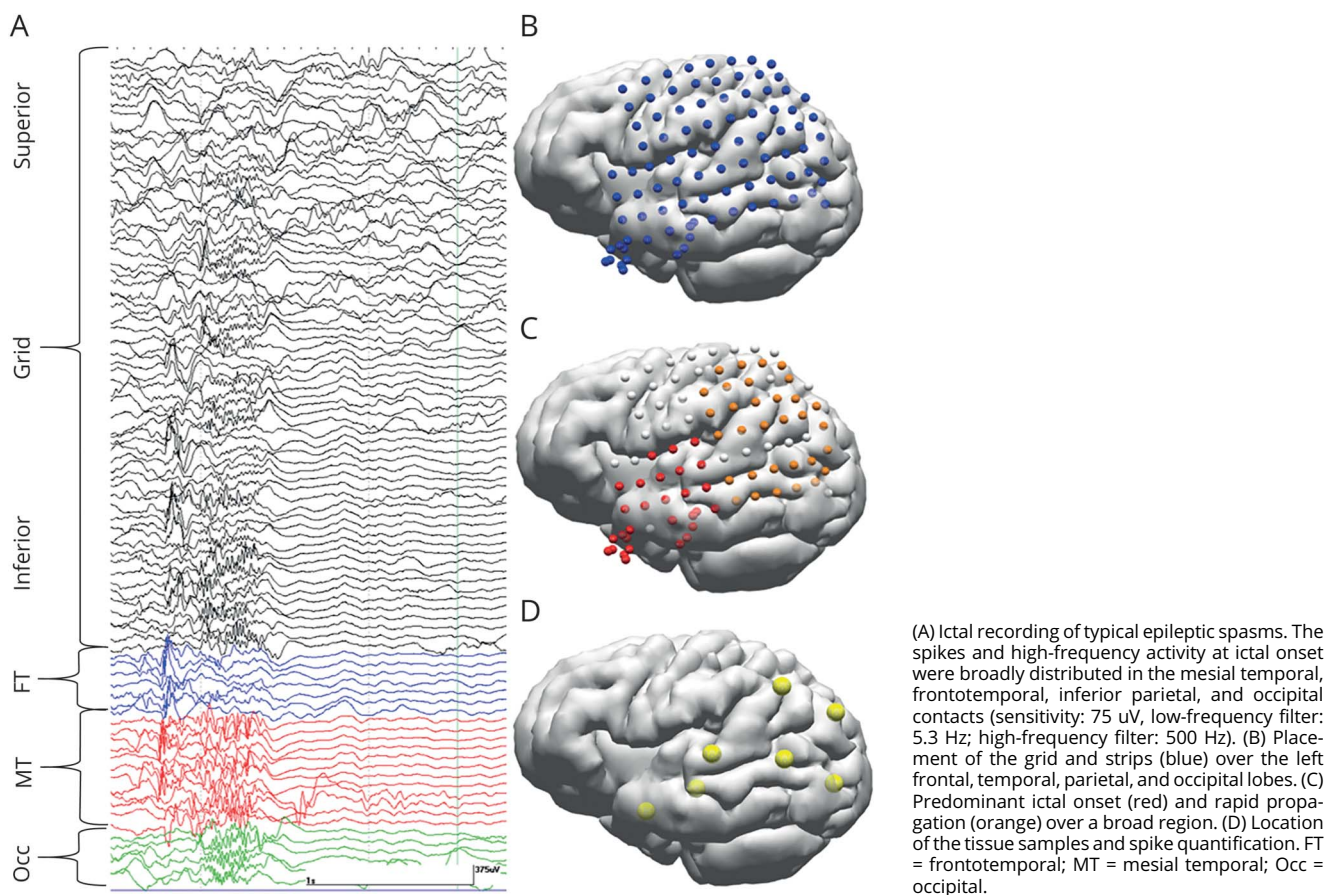
Results

Disease presentation and clinical findings

The patient is a 3-year-old male who presented at age 9 months with West syndrome, a severe form of epilepsy characterized by infantile spasms, an abnormal EEG pattern termed hypsarrhythmia, and developmental delay. The etiologies for West syndrome are multifactorial and may include genetic or structural abnormalities.[20] A commercially available epilepsy-specific gene panel using patient blood did not identify any pathogenic variants, and the patient's initial structural brain MRI was normal. His EEG revealed hypsarrhythmia with a left posterior quadrant predominance of epileptiform activity and generalized epileptic spasms. He was treated with adrenocorticotropin hormone with initial remission, followed 5 months later by recurrence and remission with prednisolone therapy. At age 2.5 years, epileptic spasms recurred along with focal tonic seizures, which were refractory to several different antiseizure medications. At that time, he underwent long-term EEG monitoring, FDG-PET, MRI, and neurodevelopmental testing as part of an evaluation for refractory seizures. New findings included seizures with left posterior quadrant onset seizures, a brain MRI finding suggestive of a temporal lobe dysplasia, and FDG-PET hypometabolism in the left temporoparietal region. This was followed by placement of subdural grids and strips covering the left posterior frontal, temporal, parietal, and occipital lobes. Ictal findings, defined as spike and wave and gamma frequency activity, were diffuse in the electrodes over the left temporal and parieto-occipital regions, including the mesial temporal contacts (figure 1). A gradient was present in the interictal epileptiform activity, where spikes were nearly

---

Figure 1 Epileptic spasm and intracranial grid location

(A) Ictal recording of typical epileptic spasms. The spikes and high-frequency activity at ictal onset were broadly distributed in the mesial temporal, frontotemporal, inferior parietal, and occipital contacts (sensitivity: 75 uV, low-frequency filter: 5.3 Hz; high-frequency filter: 500 Hz). (B) Placement of the grid and strips (blue) over the left frontal, temporal, parietal, and occipital lobes. (C) Predominant ictal onset (red) and rapid propagation (orange) over a broad region. (D) Location of the tissue samples and spike quantification. FT = frontotemporal; MT = mesial temporal; Occ = occipital.

continuous or abundant in the contacts over the hippocampus and temporal lobe contacts and frequent or occasional in contacts over the parietal and portions of the occipital lobe. Because of the diffuse nature of the ictal pattern involving the left posterior quadrant, the patient underwent a grid-based resection of presumed epileptic zones, including removal of the left temporal lobe, left amygdala, left hippocampus, left inferior parietal lobe, and left occipital lobe (table e-1, links. lww.com/NXG/A273). Histologic examination of the resected tissue specimens showed cortical dyslamination with areas featuring neurons arranged in microcolumns (occipital lobe) and areas with ill-defined hexalaminar architecture (temporal and occipital lobes), consistent with FCD type 1c according to the International League Against Epilepsy classification system.[11] The amygdala and hippocampus showed fragments of gray and white matter with gliosis. In summary, figure 2 shows neuroimaging, EEG, and histopathology of 2 vastly differentially affected brain regions, the hippocampus and occipital lobe.

Exome sequencing of brain tissues reveals somatic mosaicism in SLC35A2

DNA was extracted from 6 brain tissues from different regions within the same patient brain and from peripheral blood mononuclear cells as a matched comparator. All brain tissues were from suspected affected areas and resected during the same surgery. We performed exome sequencing initially on the 6 brain tissues plus matched blood to search for inherited (germline) variation and acquired (somatic) variation in coding regions, including single nucleotide, insertion/deletion, and copy number variants. For the temporal lobe and occipital lobe, we sequenced 2 different samples removed from the same brain region. Mean, on-target exome sequencing read coverage depth was 222x for matched blood and 331x (range: 282x–384x) for brain tissues (table e-2, links.lww.com/ NXG/A273). Our analysis of inherited variants yielded 3 variants that merited further review (table e-3, links.lww. com/NXG/A273). Two variants were within genes unrelated to the patient's phenotype. The third variant was in *DYNC1H1* and was previously identified in our patient, as well as the patient's unaffected mother, through clinical genetic testing and reported as a variant of unknown significance (VUS). De novo variants in *DYNC1H1* have been identified in individuals with malformations of cortical development and in individuals with epileptic encephalopathies, including West syndrome.[21,22] Because of the inherited status of this variant, we do not believe that it is associated with the patient's phenotype and assessed it as a VUS.

Figure 2 Neuroimaging, EEG, and histopathology of differentially affected hippocampus and parietal/occipital lobe
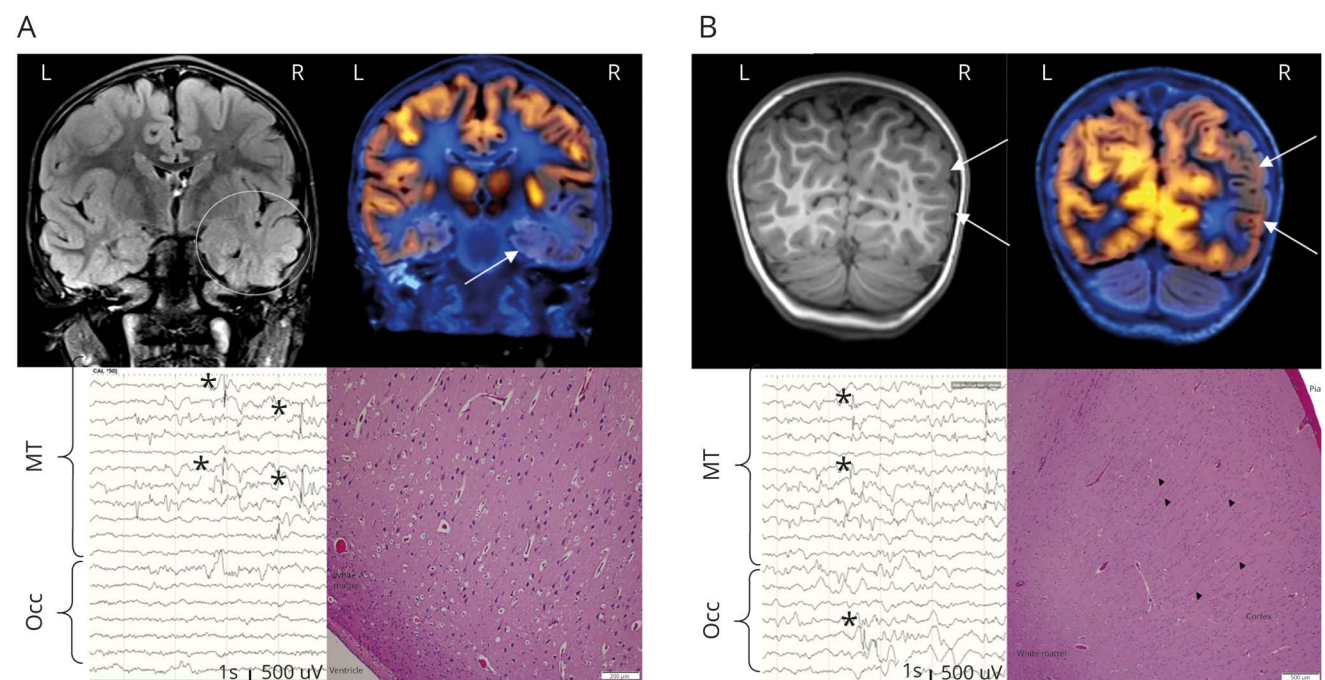
(A) Hippocampus: T2-weighted coronal MRI of the brain demonstrates increased signal within the left temporal white matter with circling of the asymmetric gray-white matter blurring on the left temporal lobe (top left). FDG-PET fused with MRI demonstrates focal area of asymmetrically decreased uptake within the left temporal lobe and hippocampus area; arrows point to the left temporal lobe and left hippocampal region (top right). Intracranial EEG demonstrates high-amplitude spikes (asterisks) abundantly in the hippocampus contacts (bottom left). Histology image at 100×; H&E-stained section from hippocampus shows expected cytoarchitecture (bottom right). (B) Parietal/occipital lobe: T1-weighted coronal MRI of the brain demonstrates no focal abnormality in the left parietal lobe (top left). FDG-PET fused with MRI demonstrates focal area of asymmetrically decreased uptake within the left parietal lobe; arrows point to the left parietal lobe (top right). Intracranial EEG demonstrates high-amplitude spikes (asterisks) only occasionally in the occipital contacts (bottom left). Histology image at 40×; H&E-stained section shows cortical dyslamination with neurons of the occipital neocortex arranged in microcolumns (arrowheads). FDG = fluorodeoxyglucose; H&E = hematoxylin and eosin.

Table 1 Variant allele fractions and annotation of somatic *SLC35A2* c.634_635delTC variant identified in the patient brain

Chrom	Position (hg19)	Gene	HGVS	Matched blood		Temporal lobe A1		Temporal lobe A2		Amygdala B		Hippocampus C		Occipital lobe D1		Occipital lobe D2	
				Depth	VAF	Depth	VAF	Depth	VAF	Depth	VAF	Depth	VAF	Depth	VAF	Depth	VAF
X	48762550	*SLC35A2*	NM_005660.3:c.634_635delTC p.Ser212LeufsTer9	108	0.00%	135	3.00%	184	3.30%	184	12.50%	206	27.70%	153	9.80%	166	0.60%

Abbreviations: Chrom = chromosome; HGVS = Human Genome Variation Society standard nomenclature; VAF = variant allele fraction.
Genomic coordinates reflect human reference genome build GRCh37.

Our analysis of acquired, somatic variants revealed 46 variants that met the initial filtering criteria, but after manually reviewing these in the IGV to discount strand bias or other sequencing artifacts, we determined that 41/46 suspect variants were sequencing artifacts. The 5 remaining candidate somatic mosaic variants are listed in table e-4, links.lww.com/NXG/A273. We identified a likely causal variant in the solute carrier family 35 member A2 (*SLC35A2*) gene, which was absent in the matched blood comparator and present in a range of VAFs from 0.6% to 27.7% in the resected brain tissues (table 1). The X-linked NM_005660.3:c.634_635delTC (p.Ser212LeufsTer9) variant is predicted to cause a frameshift in the transmembrane domain and a premature stop codon 9 amino acid downstream. This variant has not been reported in the Genome Aggregation Database of 150,647 alleles from the general population.[23] We found 1 report of this somatic variant in a patient with intractable epilepsy.[24] We assessed the p.Ser212LeufsTer9 variant as pathogenic according to the ACMG/AMP guidelines by assigning the following criteria as evidence of pathogenicity: PVS1 (null variant in a gene where loss of function is a known mechanism of disease), PS2 (de novo variant in a patient with the disease and no family history; applied due to proven somatic mosaicism), and PM2 (absence from large-scale control population databases).[15]

Deep, targeted sequencing of SLC35A2 confirms a wide range of VAFs in patient brain tissue

We used 2 different targeted sequencing approaches to confirm the *SLC35A2* variant in DNA from 6 resected brain regions and to produce high-depth sequencing data at the variant site as a means of correlating the prevalence of the variant in the cells obtained from each region. First, we used a PCR-based approach (libricon) to selectively amplify a ~100 bp region that included the variant of interest and constructed a library from the resulting amplicons. Our second variant confirmation approach included a custom direct sequencing panel NND, designed to capture and sequence all coding regions of the *SLC35A2* gene. Both targeted approaches confirmed the presence of the *SLC35A2* variant at varying proportions in different brain tissues (figure 3A).

The NND approach revealed variant read percentages ranging from 4.2% to 19.5%, which were highly similar to our initial exome sequencing allele percentages (figure 3A). NND uses UMIs added before PCR amplification, permitting the identification and removal of PCR duplicates after sequencing. Therefore, on the basis of these assay attributes, we chose NND as the methodology to confirm the *SLC35A2* variant in 6 additional brain tissues, which had been archived in FFPE blocks from the patient's initial surgery. The variant was present in all 6 additional brain tissues at a range of percentages (figure 3B). Overall, the hippocampus tissue (section C) had the highest proportion of the *SLC35A2* variant allele, whereas portions of the occipital lobe (sections D2 and F) were among the lowest proportions.
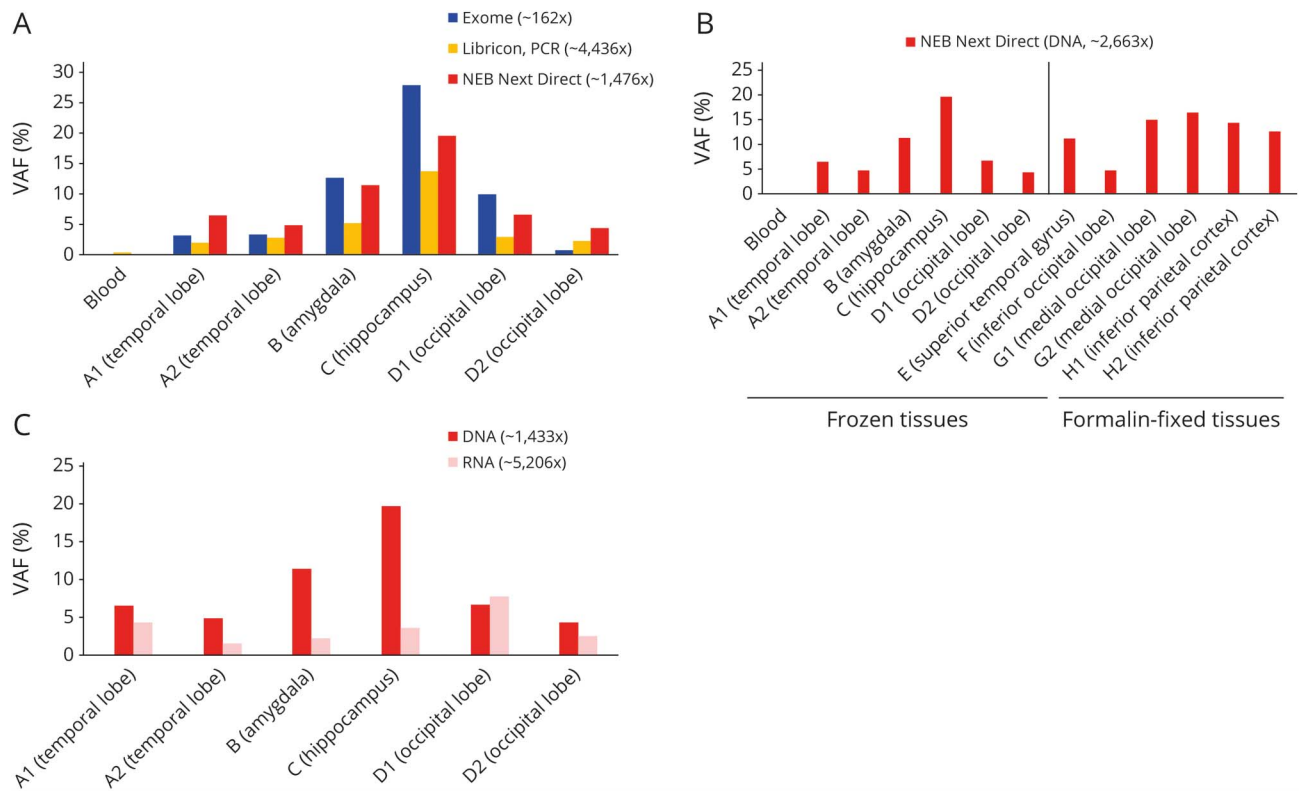
(A) Comparison of SLC35A2 c.634_635delTC VAFs in 6 brain tissues and blood comparator from the affected patient, using 3 different sequencing techniques. Average sequencing depth at the SLC35A2 variant position for each method is shown in parentheses in legend. The apparent presence of the variant at <1% VAF in the blood sample for the libricon approach is likely due to the high error rate of this PCR-based approach and the high read depth achieved during sequencing. (B) VAFs in 12 brain and 1 matched blood tissue using the NND SLC35A2 targeted sequencing kit. (C) Comparison of VAFs in DNA and RNA from 6 different brain tissues using the NND SLC35A2 targeted sequencing kit. Only nucleic acids from high-quality, frozen tissue samples were used for targeted RNA sequencing. Average sequencing depth for each method is shown in parentheses in legends. NND = NEBNext Direct; VAF = variant allele fraction.

Our initial transcriptome sequencing of total RNA yielded low read depth at the *SLC35A2* c.634_635delTC variant site. In addition, the expression level of *SLC35A2* in all brain tissues was very low. FPKM values for *SLC35A2* expression ranged from 3.2 to 3.9 across all tissues. As such, we were unable to correlate variant expression from transcriptome sequencing to the observed variability in allele proportions from the DNA data. Therefore, we performed deep sequencing using the NND targeted panel on brain-extracted RNA from 6 of the brain regions to determine whether the c.634_635delTC variant is expressed. Average read depth in RNA at the variant site was 5,206x for all tissues, and the VAF varied from 1.5% to 7.7%, demonstrating much lower proportions than were detected from DNA sequencing (figure 3C). There was no clear correlation between DNA and RNA VAFs among all tissues.

Somatic SLC35A2 VAF correlates with severity of electrophysiologic and radiographic findings

The *SLC35A2* VAF, based on high-depth NND targeted sequencing of 12 brain regions obtained at surgery, ranged from 4.2% (occipital lobe, section D2) to 19.5% (hippocampus, section C). As shown previously in figure 2,

intracranial EEG was consistent with seizure onset from the hippocampus, which had the highest VAF, but showed only occasional seizure onset from the occipital lobe, one of the lowest VAFs. This observation prompted us to quantify interictal epileptiform discharges (spikes) for all involved tissues (table 2). Average spikes per minute, a standard measure of the severity of abnormal neurophysiologic activity, correlated with the proportions of *SLC35A2* variant allele in these different brain tissues (Pearson r = 0.881, *p* = 0.0087), with the highest rate of interictal epileptiform discharges (32.8 spikes/min) observed in the tissue with the highest VAF (hippocampus, 19.5%). In addition, as shown in table 2, the trend in correlation between VAFs and IED activity is reflected in a binary descriptor of seizure onset relative to brain region and to imaging-based analyses from MRI and FDG-PET neuroimaging modalities. Electrophysiologic and neuroimaging findings generally correlated with higher VAF compared with tissues with a lower VAF, suggesting that the presence of the somatic mosaic *SLC35A2* variant is contributing to the seizure phenotype. We compare these clinical findings with findings from a previously published patient with the same *SLC35A2* somatic variant in table 3.

Table 2 Clinical phenotypic observations of all brain tissues

	Hippocampus	Superior temporal gyrus	Amygdala	Inferior parietal cortex	Temporal lobe	Superior occipital gyrus	Inferior occipital gyrus	Medial occipital lobe
Section_ID	C	E	B	H1/H2	A1/A2	F	D1/D2	G1/G2
Spikes per minute	32.8	25.3	24.3	18.8	13.8	13.7	5.7	n/a
Seizure onset	Yes	Yes	Yes	Yes	Yes	No	No	n/a
MRI	Abnormal	Abnormal	Abnormal	Normal	Abnormal	Normal	Normal	Normal
FDG-PET	Abnormal	Abnormal	Abnormal	Abnormal	Abnormal	Normal	Normal	Normal
DNA VAF (NND)	19.5%	11.1%	11.3%	12.5%–14.3%	4.8%–6.4%	4.8%	4.2%–6.5%	14.8–16.4%
RNA VAF (NND)	3.5%	n/a	2.2%	n/a	1.5%–4.2%	n/a	2.4%–7.7%	n/a
DNA VAF (exome)	27.7%	n/a	12.5%	n/a	3.0%–3.3%	n/a	0.6%–9.8%	n/a

Abbreviations: FDG = fluorodeoxyglucose; n/a = not applicable; NND = NEBNext Direct; VAF = variant allele fraction.
Various clinical observations are listed for each brain tissue alongside the corresponding *SLC35A2* c.634_635delTC VAFs detected in each specimen.

Discussion

Our comparative analysis of electrophysiologic, radiographic, histopathologic, and genomic data from multiple brain regions following left temporo-parieto-occipital resection in a patient with West syndrome has illustrated a novel finding. We identified a somatic *SLC35A2* variant p.Ser212LeufsTer9, which was detected initially by exome sequencing (VAF: 0.6%–27.7%) and confirmed with targeted gene sequencing (VAF: 4.2%–19.5%) in various affected brain tissues but not in blood. This same variant was previously reported as a somatic variant in the brain of an individual with FCD Ia.[24] Similar to the previously published patient, brain specimens harboring the mosaic *SLC35A2* variant from our patient showed cortical dyslamination, FCD type 1c, suggesting that the somatic variant is associated with pathogenesis. A germline de novo variant (p.Tyr145ProfsTer76), which results in truncation at the same amino acid (p.221) as our variant, was reported in a patient with EOEE and West syndrome.[25] The authors demonstrated

Table 3 Comparison of clinical features in our patient compared with a previously published patient with identical brain somatic *SLC35A2* c.634_635delTC variant

	Our patient	Published case[25]
Variant	p.Ser212LeufsTer9 (somatic)	p.Ser212LeufsTer9 (somatic)
VAF	Somatic: 0.6%–27.7% (exome sequencing); 4.2%–19.5% (targeted sequencing)	Somatic: 14.3% (exome sequencing); 6.8% (targeted sequencing)
Diagnosis/ seizure type	West syndrome	Focal epilepsy
Age at onset/sex	Male/9 mo	Male/17 y
Preoperative MRI	Abnormal temporal lobe (underrepresentative of the dysplasia)	Normal
Pathology	FCD1c with varying degrees of cortical dyslamination and some gyri "small with complex configurations"	FCD1a, hypercellular
Hypsarrhythmia/ EIEE	Yes	No
Location	Left posterior temporal-occipital lobe (nondominant)	Right posterior temporal-occipital lobe (nondominant)

Abbreviations: EIEE = early infantile epileptic encephalopathy; FCD = focal cortical dysplasia; VAF = variant allele fraction.
Various clinical observations are listed for our patient and for a previously published patient who was reported to have the same somatic variant as our patient.[25]

through in vitro cell culture studies using a mouse cell line that the p.Tyr145ProfsTer76 mutant expression was severely diminished. A comparison of *SLC35A2* expression in brain tissues from our patient revealed that expression is indeed diminished compared with brain tissues from other patients with epilepsy (figure e-2, links.lww.com/NXG/A273). Likewise, results from targeted sequencing in our patient affected brain tissues revealed the variant was estimated at much lower read percentage in RNA than in DNA, suggesting a nonsense-mediated decay (NMD) mechanism. Clear correlation between DNA variant allele and RNA VAFs or RNA expression within each tissue was not observed. However, NMD is a dynamic process, and the extracted and sequenced RNA represents only a snapshot of what is occurring in cells at any given time point. Therefore, NMD is likely the reason for low expression of the variant allele in RNA and lower expression of *SLC35A2* transcripts compared with other patients. We predict that overall SLC35A2 protein levels would be diminished in the patient brain and therefore would associate with pathogenesis and the patient phenotype.

The *SLC35A2* gene encodes for a protein which transports uridine-diphosphate-galactose from the cytosol to the Golgi, where it functions in asparagine (N-linked) glycosylation, an essential post-translational modification of proteins. Studies in mice revealed genetic inactivation of key components of the N-glycosylation pathway resulted in various neurologic defects.[26,27] Recessive conditions involving glycosylation defects in humans (e.g., *PMM2*, *ALG6*, and *SRD5A3*) lead to a variety of clinical features, most often neurologic symptoms.[28–30] Individuals born with inherited genetic defects in the N-glycosylation pathway often present with severe neurologic abnormalities including seizures, epileptic encephalopathy, and cerebellar hypoplasia. In particular, heterozygous variants in the X-linked *SLC35A2* in females are associated with congenital disorder of glycosylation Type IIm and are characterized by infantile-onset seizures, hypsarrhythmia, severe intellectual disability, and hypotonia.[25,31,32] In addition to inherited germline variants, previous studies have reported, similar to our patient, identification of mosaic variants in *SLC35A2* as a cause of early-onset epileptic encephalopathy, FCD and nonlesional focal epilepsy.[24,32,33] A plot of all pathogenic and likely pathogenic germline and somatic *SLC35A2* coding variants reported in ClinVar is shown in figure e-3, links.lww.com/NXG/A273.

Our group used an integrated combination of conventional approaches (radiology, histopathology, and electrophysiology) plus high-depth NGS to comprehensively analyze multiple brain tissues from a single patient with intractable epilepsy. Our sequencing results reveal that the *SLC35A2* variant affects RNA expression and is therefore likely associated with the patient phenotype. In concordance with this conclusion, the proportionality of the mosaicism of the *SLC35A2* variant in various brain regions correlated with the severity of neurophysiologic and presence or absence of radiographic abnormalities. Although low prevalence of the

SLC35A2 variant allele still was sufficient to cause FCD pathology, some tissues with low-level variant fractions appeared to be unaffected according to neuroimaging and onset of seizure activity, suggesting a potential threshold effect for epileptogenesis. Furthermore, the amygdala and hippocampus did not have apparent histologic pathology on initial examination. Yet, the hippocampus and amygdala regions were determined to be among the most epileptogenic regions in this patient, highlighting the strength of our study to verify underlying focal epileptogenic abnormalities using molecular pathology (i.e., DNA sequencing) in histologically normal tissue. Collectively, our findings support the understudied association of brain somatic mosaicism with intractable epilepsy and reinforce the need for studies that use a combination of clinical data analysis alongside deep NGS of affected brain tissue as a means to identify underlying aspects of genetic pathogenicity.

Appendix Authors

Name	Location	Contribution
Katherine E. Miller, PhD	Nationwide Children's Hospital, Columbus, OH	Design and conceptualization of the study; analysis and interpretation of genomic data; and drafted the initial manuscript
Daniel C. Koboldt, MS	Nationwide Children's Hospital; The Ohio State University, Columbus, OH	Design and conceptualization of the study; analysis and interpretation of genomic data; and revised the manuscript for intellectual content
Kathleen M. Schieffer, PhD	Nationwide Children's Hospital, Columbus, OH	Analysis and interpretation of genomic data and revised the manuscript for intellectual content

Continued

Appendix *(continued)*

Name	Location	Contribution
Tracy A. Bedrosian, PhD	Nationwide Children's Hospital, Columbus, OH	Analysis and interpretation of genomic data and revised the manuscript
Erin Crist, MMSc, LGC	Nationwide Children's Hospital, Columbus, OH	Major role in acquisition of data
Adrienne Sheline, MPH	Nationwide Children's Hospital, Columbus, OH	Major role in acquisition of data
Kristen Leraas, MS	Nationwide Children's Hospital, Columbus, OH	Major role in acquisition of data
Vincent Magrini, PhD	Nationwide Children's Hospital; The Ohio State University, Columbus, OH	Design and conceptualization of the study; analysis and interpretation of genomic data; and revised the manuscript for intellectual content
Huachun Zhong, MS	Nationwide Children's Hospital, Columbus, OH	Major role in acquisition of data
Patrick Brennan, MS	Nationwide Children's Hospital, Columbus, OH	Major role in acquisition of data
Jocelyn Bush, MS	Nationwide Children's Hospital, Columbus, OH	Major role in acquisition of data
James Fitch, BS	Nationwide Children's Hospital, Columbus, OH	Major role in acquisition of data
Natalie Bir, BS	Nationwide Children's Hospital, Columbus, OH	Major role in acquisition of data
Anthony R. Miller, PhD	Nationwide Children's Hospital, Columbus, OH	Major role in acquisition of data
Catherine E. Cottrell, PhD	Nationwide Children's Hospital; The Ohio State University, Columbus, OH	Design and conceptualization of the study; analysis and interpretation of genomic data; and revised the manuscript for intellectual content
Jeffrey Leonard, MD	Nationwide Children's Hospital; The Ohio State University, Columbus, OH	Major role in acquisition of data
Jonathan A. Pindrik, MD	Nationwide Children's Hospital; The Ohio State University, Columbus, OH	Major role in acquisition of data
Jerome A. Rusin, MD	Nationwide Children's Hospital, Columbus, OH	Major role in acquisition of data and analysis and interpretation of clinical data
Summit H. Shah, MD, MPH	Nationwide Children's Hospital, Columbus, OH	Major role in acquisition of data and analysis and interpretation of clinical data
Peter White, PhD	Nationwide Children's Hospital; The Ohio State University, Columbus, OH	Design and conceptualization of the study; major role in acquisition of data; and analysis and interpretation of genomic data

Appendix *(continued)*

Name	Location	Contribution
Richard K. Wilson, PhD	Nationwide Children's Hospital; The Ohio State University, Columbus, OH	Design and conceptualization of the study
Elaine R. Mardis, PhD	Nationwide Children's Hospital; The Ohio State University, Columbus, OH	Design and conceptualization of the study; analysis and interpretation of genomic data; and revised the manuscript for intellectual content
Christopher R. Pierson, MD, PhD	Nationwide Children's Hospital; The Ohio State University, Columbus, OH	Major role in acquisition of data; analysis and interpretation of clinical data; and revised the manuscript for intellectual content
Adam P. Ostendorf, MD	Nationwide Children's Hospital; The Ohio State University, Columbus, OH	Major role in acquisition of data; analysis and interpretation of clinical data; and drafted the initial manuscript

References

1. Carvill GL, Regan BM, Yendle SC, et al. GRIN2A mutations cause epilepsy-aphasia spectrum disorders. Nat Genet 2013;45:1073–1076.
2. Claes L, Del-Favero J, Ceulemans B, Lagae L, Van Broeckhoven C, De Jonghe P. De novo mutations in the sodium-channel gene SCN1A cause severe myoclonic epilepsy of infancy. Am J Hum Genet 2001;68:1327–1332.
3. Singh NA, Charlier C, Stauffer D, et al. A novel potassium channel gene, KCNQ2, is mutated in an inherited epilepsy of newborns. Nat Genet 1998;18:25–29.
4. Schuele SU, Luders HO. Intractable epilepsy: management and therapeutic alternatives. Lancet Neurol 2008;7:514–524.
5. Dwivedi R, Ramanujam B, Chandra PS, et al. Surgery for drug-resistant epilepsy in children. N Engl J Med 2017;377:1639–1647.
6. Kwan P, Brodie MJ. Early identification of refractory epilepsy. N Engl J Med 2000; 342:314–319.
7. Lee JH, Huynh M, Silhavy JL, et al. De novo somatic mutations in components of the PI3K-AKT3-mTOR pathway cause hemimegalencephaly. Nat Genet 2012;44: 941–945.
8. Moller RS, Weckhuysen S, Chipaux M, et al. Germline and somatic mutations in the MTOR gene in focal cortical dysplasia and epilepsy. Neurol Genet 2016;2:e118.
9. Lim JS, Kim WI, Kang HC, et al. Brain somatic mutations in MTOR cause focal cortical dysplasia type II leading to intractable epilepsy. Nat Med 2015;21:395–400.
10. Dobin A, Davis CA, Schlesinger F, et al. STAR: ultrafast universal RNA-seq aligner. Bioinformatics 2013;29:15–21.
11. Blumcke I, Thom M, Aronica E, et al. The clinicopathologic spectrum of focal cortical dysplasias: a consensus classification proposed by an ad hoc Task Force of the ILAE Diagnostic Methods Commission. Epilepsia 2011;52:158–174.
12. Kelly BJ, Fitch JR, Hu Y, et al. Churchill: an ultra-fast, deterministic, highly scalable and balanced parallelization strategy for the discovery of human genetic variation in clinical and population-scale genomics. Genome Biol 2015;16:6.
13. DePristo MA, Banks E, Poplin R, et al. A framework for variation discovery and genotyping using next-generation DNA sequencing data. Nat Genet 2011;43: 491–498.
14. Cibulskis K, Lawrence MS, Carter SL, et al. Sensitive detection of somatic point mutations in impure and heterogeneous cancer samples. Nat Biotechnol 2013;31: 213–219.
15. Richards S, Aziz N, Bale S, et al. Standards and guidelines for the interpretation of sequence variants: a joint consensus recommendation of the American College of Medical Genetics and Genomics and the Association for Molecular Pathology. Genet Med 2015;17:405–424.
16. Love MI, Huber W, Anders S. Moderated estimation of fold change and dispersion for RNA-seq data with DESeq2. Genome Biol 2014;15:550.
17. Emerman AB, Bowman SK, Barry A, et al. NEBNext direct: a novel, rapid, hybridization-based approach for the capture and library conversion of genomic regions of interest. Curr Protoc Mol Biol 2017;119:7 30 31–37 30 24.
18. Koboldt DC, Zhang Q, Larson DE, et al. VarScan 2: somatic mutation and copy number alteration discovery in cancer by exome sequencing. Genome Res 2012;22: 568–576.

19. Li H. A statistical framework for SNP calling, mutation discovery, association mapping and population genetical parameter estimation from sequencing data. Bioinformatics 2011;27:2987–2993.

20. Wirrell EC, Shellhaas RA, Joshi C, et al. How should children with West syndrome be efficiently and accurately investigated? Results from the National Infantile Spasms Consortium. Epilepsia 2015;56:617–625.

21. Poirier K, Lebrun N, Broix L, et al. Mutations in TUBG1, DYNC1H1, KIF5C and KIF2A cause malformations of cortical development and microcephaly. Nat Genet 2013;45:639–647.

22. Lin Z, Liu Z, Li X, et al. Whole-exome sequencing identifies a novel de novo mutation in DYNC1H1 in epileptic encephalopathies. Sci Rep 2017;7:258.

23. Lek M, Karczewski KJ, Minikel EV, et al. Analysis of protein-coding genetic variation in 60,706 humans. Nature 2016;536:285–291.

24. Winawer MR, Griffin NG, Samanamud J, et al. Somatic SLC35A2 variants in the brain are associated with intractable neocortical epilepsy. Ann Neurol 2018;83:1133–1146.

25. Kodera H, Nakamura K, Osaka H, et al. De novo mutations in SLC35A2 encoding a UDP-galactose transporter cause early-onset epileptic encephalopathy. Hum Mutat 2013;34:1708–1714.

26. Ye Z, Marth JD. N-glycan branching requirement in neuronal and postnatal viability. Glycobiology 2004;14:547–558.

27. Thiel C, Korner C. Mouse models for congenital disorders of glycosylation. J Inherit Metab Dis 2011;34:879–889.

28. Cantagrel V, Lefeber DJ, Ng BG, et al. SRD5A3 is required for converting polyprenol to dolichol and is mutated in a congenital glycosylation disorder. Cell 2010;142:203–217.

29. Imbach T, Grunewald S, Schenk B, et al. Multi-allelic origin of congenital disorder of glycosylation (CDG)-Ic. Hum Genet 2000;106:538–545.

30. Freeze HH, Eklund EA, Ng BG, Patterson MC. Neurology of inherited glycosylation disorders. Lancet Neurol 2012;11:453–466.

31. Kimizu T, Takahashi Y, Oboshi T, et al. A case of early onset epileptic encephalopathy with de novo mutation in SLC35A2: clinical features and treatment for epilepsy. Brain Dev 2017;39:256–260.

32. Ng BG, Buckingham KJ, Raymond K, et al. Mosaicism of the UDP-galactose transporter SLC35A2 causes a congenital disorder of glycosylation. Am J Hum Genet 2013;92:632–636.

33. Sim NS, Seo Y, Lim JS, et al. Brain somatic mutations in SLC35A2 cause intractable epilepsy with aberrant N-glycosylation. Neurol Genet 2018;4:e294.